Journal of The Korean Astronomical Society
46: 33 ∼ 40, 2013 February

http://dx.doi.org/10.5303/JKAS.2013.46.1.33
ISSN:1225-4614
http://jkas.kas.org

HOT GAS HALOS IN EARLY-TYPE GALAXIES AND ENVIRONMENTS

Eunbin Kim[1], Yun-Young Choi[2], & Sungsoo S. Kim[1,2]
[1] School of Space Research, Kyung Hee University, Yongin, Gyeonggi 446-701, Korea
E-mail: ebkim@khu.ac.kr
[2] Department of Astronomy & Space Science, Kyung Hee University, Gyeonggi 446-701, Korea
E-mail: yy.choi@khu.ac.kr
(Received October 5, 2009; Revised December 4, 2012; Accepted December 15, 2012)

ABSTRACT

We investigate the dependence of the extended X-ray emission from the halos of optically luminous early-type galaxies on the small-scale (the nearest neighbor distance) and large-scale (the average density inside the 20 nearest galaxies) environments. We cross-match the 3rd Data Release of the Second *XMM-Newton* Serendipitous Source Catalog (2XMMi-DR3) to a volume-limited sample of the Sloan Digital Sky Survey (SDSS) Data Release 7 with $M_r < -19.5$ and $0.020 < z < 0.085$, and find 20 early-type galaxies that have extended X-ray detections. The X-ray luminosity of the galaxies is found to have a tighter correlation with the optical and near infrared luminosities when the galaxy is situated in the low large-scale density region than in the high large-scale density region. Furthermore, the X-ray to optical (r-band) luminosity ratio, L_X/L_r, shows a clear correlation with the distance to the nearest neighbor and with large-scale density environment only where the galaxies in pair interact hydrodynamically with seperations of $r_p < r_{\rm vir}$. These findings indicate that the galaxies in the high local density region have other mechanisms that are responsible for their halo X-ray luminosities than the current presence of a close encounter, or alternatively, in the high local density region the cooling time of the heated gas halo is longer than the typical time between the subsequent encounters.

Key words : galaxies: halos — X-rays: galaxies — galaxies: elliptical and lenticular

1. INTRODUCTION

Since the *Einstein* observatory discovered the existence of an extended hot gas halo in early-type galaxies (Forman et al. 1985; Trinchieri & Fabbiano 1985), X-ray observations have made great progress in understanding the origin, evolution, and nature of hot gas in early-type galaxies. Previous studies have shown that the X-ray luminosity of early-type galaxies correlates with optical luminosity in a manner that exhibits a transition with varying optical luminosity and large scatters around the correlation (Canizares et al. 1987; Eskridge et al. 1995; Brown & Bregman 1998; O'Sullivan et al. 2001; Ellis & O'Sullivan 2006). The correlation suggests that the hot halo gas may be related to gas ejected from evolving stars and planetary nebulae inside the early-type galaxy (Mathews 1990; Mathews & Brighenti 2003; Bregman & Parriott 2009). The large scatter in the correlation especially found in more luminous early-type galaxies has been often explained in terms of externally driven processes (White & Sarazin 1991; Brown & Bregman 2000). The relative importance of particular processes varies with environment where galaxies reside. The hot gas halo can be stripped when a galaxy enters a group or cluster (White & Frenk 1991), and hot halo in galaxies embedded in intragroup medium can be even enhanced (Canizares et al. 1983). On the other hand, other researchers found no such correlation between the X-ray and optical/near-infrared (NIR) luminosities and environments (O'Sullivan et al. 2001; Helsdon et al. 2001; Ellis & O'Sullivan 2006).

Recently, the high spatial resolution of *Chandra* or *XMM-Newton* allows one to cleanly separate out the thermal emission in the hot halo gas from other contributions such as active galactic nuclei (AGNs) and X-ray binaries (Silverman et al. 2005; Kim & Fabbiano 2010) or the more extended intragroup or cluster medium. Detailed studies of the X-ray/optical relation in diverse environments has shown us that the environmental processes could be important in addition to internal processes (Memola et al. 2009; Mulchaey & Jeltema 2010; Sun et al. 2007; Jeltema et al. 2008; Rasmussen et al. 2012).

It has been found that galaxy properties such as morphology, luminosity, star formation rate (SFR) and AGN activity strongly depend on the distance to the nearest neighbor galaxy, and this indicates that the hydrodynamical interactions between neighboring galaxies play an important role in determining galaxy properties (Park et al. 2008; Park & Choi 2009; Hwang & Park 2009, 2010; Hwang et al. 2010, 2011). Thus it is natural to infer that the neighbor galaxies play a role in the presence of a hot gas halo in early-type galaxies.

In this paper, by using a sample cross-matched be-

Table 1.
Basic parameters of the 20 cross-matched early-type galaxies

SDSS ID[a]	Name[a]	z[a]	$\log(\rho_{20}/\rho)$[a]	$\log(r_p/r_{\rm vir,nei})$[a]	$M_r^{\rm a}$	$M_r^{\rm b}$	Class[a,c]
SDSS J073426.44+314536.2	-	0.06044	0.862	0.414	-21.58	-21.60	*ww*AGN
SDSS J102141.22+235523.0	NGC3216	0.03925	1.363	0.965	-21.98	-21.74	*ww*SFG
SDSS J102245.51+194717.5	-	0.03890	1.126	-1.212	-20.65	-20.23	*w*AGN
SDSS J115324.36+230415.2	-	0.02672	0.811	-0.383	-20.44	-20.06	*s*Comp
SDSS J120409.40+202052.5	NGC4066	0.02457	1.892	-0.788	-21.47	-21.46	*w*AGN
SDSS J120805.55+251414.3	-	0.02264	1.308	0.666	-20.94	-20.91	*s*Comp
SDSS J121205.45+131220.2	NGC4164	0.06488	1.112	0.685	-21.98	-21.99	*ww*AGN
SDSS J122858.44+021127.1	-	0.07780	0.693	0.366	-21.50	-21.49	*w*Comp
SDSS J124100.33+183314.0	-	0.07375	1.802	0.813	-21.99	-20.96	*s*Comp
SDSS J125935.70+275733.3	NGC4874	0.02402	2.160	0.203	-21.82	-21.68	*ww*AGN
SDSS J130919.09−013721.1	-	0.08389	1.129	0.828	-22.31	-22.23	*ww*SFG
SDSS J132014.72+330836.2	NGC5098	0.03615	1.708	-1.361	-21.32	-21.23	*s*AGN
SDSS J132410.02+135835.5	NGC5129	0.02304	0.859	1.116	-21.84	-21.49	*ww*AGN
SDSS J133110.82−014348.9	-	0.08365	2.172	-1.662	-22.12	-22.17	*w*Comp
SDSS J141643.21+105307.3	NGC5531	0.02582	0.658	-0.705	-21.01	-22.10	*s*AGN
SDSS J142758.18+263016.2	-	0.03236	0.109	0.900	-21.27	-20.98	*w*AGN
SDSS J150611.68+030833.2	-	0.04247	1.004	0.950	-21.65	-21.67	*ww*SFG
SDSS J152140.12+075235.3	-	0.07648	1.545	0.441	-21.53	-21.19	*s*AGN
SDSS J160435.79+174317.6	NGC6041A	0.03533	2.063	0.333	-21.65	-21.50	*ww*AGN
SDSS J162741.13+405537.0	NGC6160	0.03173	1.929	0.313	-21.91	-21.49	*w*Comp

Notes. [a] Target Galaxy, [b] Neighbor Galaxy, [c] Spectral types of galaxies are determined by the flux ratios of Balmer and ionization lines ([OIII]/Hβ and [NII]/Hα; Baldwin et al. (1981)); *s*, *w*, and *ww* represent galaxies defined by the flux ratios with $S/N \geq 10$, $3 \leq S/N < 10$, and $S/N < 3$, respectively. SFG stands for star-forming galaxy. Composite object is denoted by 'Comp' which contain AGNs as well as extended H_{II} regions (Kauffmann et al. 2003).

tween *XMM-Newton* and SDSS DR7 (York et al. 2000; Abazajian et al. 2009), we will perform a study on the dependence of X-ray luminosity from hot halo gas in optically bright early-type galaxies on the larger-scale background density and the local density from the nearest neighbor. Section 2 describes the sample used in this study and in Section 3, we present results of the environmental dependence of the X-ray luminosities. The implications of our results are summarized and discussed in Section 4. Throughout this paper, we adopt a flat ΛCDM cosmology with $\Omega_\Lambda = 0.73$ and $\Omega_M = 0.27$.

2. SAMPLE SELECTION AND DATA ANALYSIS

2.1 The Match between SDSS Optical and *XMM-Newton* X-Ray Surveys

The Second XMM-Newton Serendipitous Source Catalogue (version 2XMMi-DR3) contains pointed observation sources and serendipitous X-ray sources near the targets. The 2XMMi-DR3 contains 353,191 detections corresponding to 262,902 unique sources. Out of these X-ray sources, 30,470 extended sources were detected and then reduced to 16,605 sources after removing spurious sources (with index `sum_flag` > 3).

A volume-limited sample of 125,524 galaxies with absolute r-band magnitude brighter than -19.5 and a redshift $0.02 < z < 0.0859$ was generated from the KIAS value-added catalog (Choi et al. 2010), which supplements the bright galaxies missing in the SDSS Main galaxy sample. For a target galaxy with absolute magnitude M_r, the nearest neighbor galaxy is the one brighter than $M_r + 0.5$ with the smallest projected separation across the line of sight from the target galaxy, and with a radial velocity difference less than 600 km s^{-1} for early-type target or 400 km s^{-1} for late-type target, respectively. For the completeness of the neighbors, we only study 73,440 target galaxies brighter than $M_r = -20.0$. The rest-frame absolute magnitudes of individual galaxies were computed in fixed bandpasses, shifted to $z = 0.1$, using Galactic reddening correction (Schlegel et al. 1998) and K-corrections as described by Blanton et al. (2003). The mean evolution correction given by Tegmark et al. (2004), $E(z) = 1.6(z - 0.1)$, was also applied.

We obtained 100 samples from the positional cross-matching between the X-ray sources and the SDSS target galaxies we selected. When more than one extended sources were cross-matched to an optical source, the source having the highest detection likelihood was chosen. Then we selected only early-type galaxies by visual inspection. There remained 48 unique X-ray sources that were matched to early-type galaxies. Out of these matches, only 20 extended sources satisfied the following three criteria (Watson et al. 2008) 1) the source should have ≥ 500 total-band EPIC counts, 2) the detector coverage of the source should be larger than 0.5 which is weighted by the point spread function for the `pn` and `MOS` cameras, 3) the total-band detection likelihood for each camera should be larger than 15. Due to the small size of the sample, interpretation of the relationships obtained from such samples would require careful analysis throughout this paper.

Table 2.
Optical/NIR/X-ray luminosities of the sample

SDSS ID	$\log(L_r/L_{r,\odot})$	$\log(L_K/L_{K,\odot})$	$\log L_X$	Model[a]
SDSS J073426.44+314536.2	10.54	11.10	$40.82^{+0.04}_{-0.03}$	mekal+power
SDSS J102141.22+235523.0	10.69	11.37	$41.12^{+0.07}_{-0.09}$	mekal
SDSS J102245.51+194717.5	10.16	10.77	$40.25^{+0.06}_{-0.04}$	mekal+power
SDSS J115324.36+230415.2	10.08	10.66	$39.92^{+0.04}_{-0.02}$	mekal+power
SDSS J120409.40+202052.5	10.49	11.07	$41.10^{+0.05}_{-0.04}$	mekal+power
SDSS J120805.55+251414.3	10.28	10.88	$> 40.33^{+0.02}_{-0.01}$	mekal+power
SDSS J121205.45+131220.2	10.69	11.24	$41.26^{+0.03}_{-0.03}$	mekal+power
SDSS J122858.44+021127.1	10.50	11.16	$40.51^{+0.07}_{-0.05}$	mekal+power
SDSS J124100.33+183314.0	10.70	11.36	$41.01^{+0.11}_{-0.05}$	mekal+power
SDSS J125935.70+275733.3	10.63	11.41	$> 40.26^{+0.02}_{-0.01}$	mekal+power
SDSS J130919.09−013721.1	10.83	11.51	$> 42.25^{+0.01}_{-0.01}$	mekal+power
SDSS J132014.72+330836.2	10.43	10.98	$> 41.63^{+0.01}_{-0.01}$	mekal+power
SDSS J132410.02+135835.5	10.64	11.26	$> 41.01^{+0.01}_{-0.01}$	mekal+power
SDSS J133110.82−014348.9	10.75	11.67	$> 41.52^{+0.02}_{-0.02}$	mekal+power
SDSS J141643.21+105307.3	10.31	10.90	$40.01^{+0.05}_{-0.04}$	mekal+power
SDSS J142758.18+263016.2	10.41	10.98	$> 40.83^{+0.02}_{-0.02}$	mekal+power
SDSS J150611.68+030833.2	10.57	11.13	$40.56^{+0.14}_{-0.09}$	mekal
SDSS J152140.12+075235.3	10.51	11.15	$40.54^{+0.13}_{-0.10}$	mekal+power
SDSS J160435.79+174317.6	10.57	11.31	$> 41.77^{+0.01}_{-0.01}$	mekal+power
SDSS J162741.13+405537.0	10.67	11.29	$41.09^{+0.04}_{-0.04}$	mekal+power

Notes. [a]The spectral fitting models. L_K values are calculated from K-band magnitudes given by the Two Micron All Sky Survey. L_X values are X-ray luminosity in 0.5-2 keV band for thermal component only in unit of ergs s^{-1}.

2.2 Environmental Parameters

We use two environmental parameters. One is the mass density, ρ_{20}, measured by using twenty nearest galaxies in the same volume-limited sample over a few Mpc scale, corresponding to large-scale environment. The other is the distance to the nearest neighbor galaxy normalized by the virial radius of the nearest neighbor, corresponding to small-scale environment.

The local density attributed to the nearest neighbor is estimated by

$$\rho_n/\bar{\rho} = 3\gamma_n L_n/4\pi r_p^3 \bar{\rho}, \quad (1)$$

where r_p is the projected separation of the nearest neighbor galaxy from the target galaxy, $\bar{\rho}$ is the mean mass density of the survey volume, γ_n is the mass-to-light ratio of the neighbor galaxy, and L_n is the r-band luminosity of the neighbor galaxy. The virial radius of a galaxy can be thus defined by the projected radius where the mean mass density, ρ_n, within the sphere with radius of r_p is 740 times the mean density, which is given by

$$r_{\rm vir} = (3\gamma_n L_n/4\pi/740\bar{\rho})^{1/3} h^{-1}{\rm Mpc}. \quad (2)$$

According to this formula, the virial radius of galaxies with $M_r = -20.0$ is about 300 h^{-1} kpc for early types. The methods of calculating ρ_{20} and $r_{\rm vir}$ are described in full detail in Park et al. (2008) and Park & Choi (2009).

Table 3.
Best fit values to the L_X *vs.* L_r/L_K relation

	r-band	
Sample	A	B
$\rho_{20}/\bar{\rho} > 20$	2.16 ± 0.99	40.88 ± 0.25
$\rho_{20}/\bar{\rho} \leq 20$	2.80 ± 0.66	40.82 ± 0.12
	K-band	
Sample	A	B
$\rho_{20}/\bar{\rho} > 20$	1.49 ± 0.57	40.67 ± 0.32
$\rho_{20}/\bar{\rho} \leq 20$	2.63 ± 0.47	40.55 ± 0.10

Notes. The best fit to the each relation of L_X-L_r and L_X-L_K is given by $\log(L_{0.5-2.0{\rm keV}}) = {\rm A}\log(L_r/10^{10.5}L_{r,\odot})$+B and $\log(L_{0.5-2.0{\rm keV}}) = {\rm A}\log(L_K/10^{11}L_{K,\odot})$+B, respectively.

Table 1 lists the environmental parameters of the 20 final early-type galaxies. The absolute magnitudes of target galaxies and their neighbors are also given.

2.3 Analysis of X-ray Data

We analysed the EPIC spectra of the 20 galaxies given by the 2XMMi-DR3 pipeline. All spectra are automatically extracted with a fixed radius of 28″, which causes underestimation of X-ray luminosity for some of our samples with thermal emission extended larger

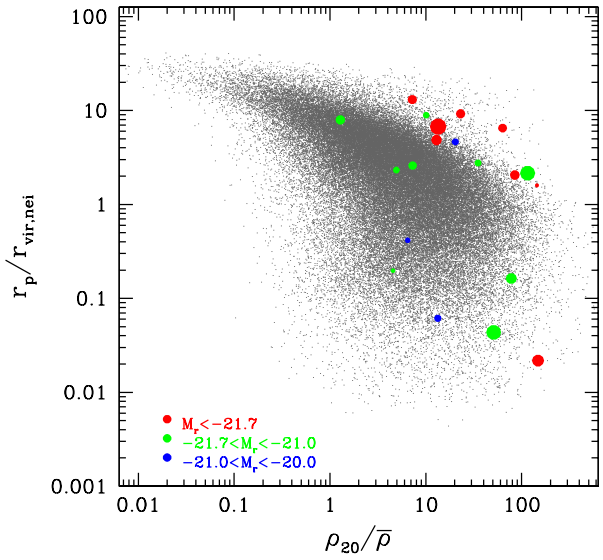

Fig. 1.— Distribution of early-type galaxies (colored solid circles) on the neighbor separation r_p and large scale background density, ρ_{20}. Gray points represent galaxies brighter than $M_r = -20.0$ in the volume-limited sample. Cases are divided into three subsamples with different optical luminosities. X-ray luminosity is proportional to the size of the circle.

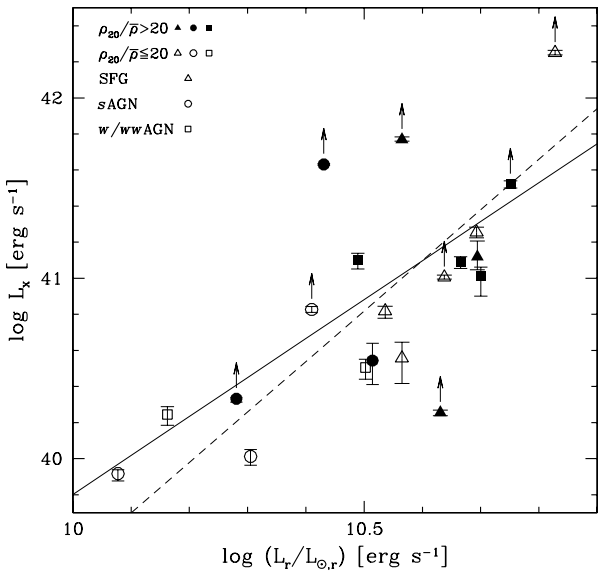

Fig. 2.— X-ray and optical (r-band) luminosity relation for galaxies in different large-scale environments. Best-fit lines are drawn for galaxies in high density region (filled symbols, solid line) and galaxies in low density region (open symbols, dashed line). Different spectral types of the galaxies are represented by different symbols: star-forming galaxies by triangles, AGNs with $S/N \geq 10$ (sAGN) by circles, and AGNs with $S/N < 10$ (wAGN and wwAGN) by squares. Composite is classified as AGN.

than the source extracting radius. Note that their X-ray luminosities listed in Table 2 are thus lower limits.

Spectral analysis was performed using the XSPEC 12.7.0. Since the hot gas sources might be contaminated with low mass X-ray binaries (LMXB) or potential AGN components, we fitted the spectra in the 0.5-7 keV band to carefully resolve their contributions as described in Jeltema et al. (2008) and Mulchaey & Jeltema (2010). To measure the unabsorbed flux of the thermal X-ray emission from the hot halo gas, a two component spectral model consisting of a thermal plasma `MEKAL` model and a power law, is adopted.

The column density was fixed as Galactic HI column density derived by using the HEASARC web-based tool* and the metallicity was fixed at $0.8Z_{\odot}$. The temperature, photon index, and spectral normalization were set to be free parameters.

For two galaxies, SDSS J150611.68+030833.2, NGC 3216, both components could not be constrained even when photon index was fixed at 1.7 (a good approximation for both low-mass X-ray binaries and AGNs). Hence we adopted only the thermal plasma model. To study the hot gas content in a galaxy, we use the luminosity only from the thermal component in the 0.5-2 keV band for comparison with other studies. Errors were determined using the Monte Carlo Markov Chains. Results from the spectral analysis and optical/NIR luminosities are listed in Table 2.

*http://heasarc.gsfc.nasa.gov/cgi-bin/Tools/w3nh/w3nh.pl

Fig. 1 shows the distribution of the 20 early-type galaxies (colored solid circles) on the r_p-$\rho_{20}/\bar{\rho}$ space. The samples are divided into three subsamples according to their absolute magnitudes. The size of the circle is proportional to the X-ray luminosity.

3. ENVIRONMENTAL DEPENDENCE OF X-RAY LUMINOSITIES

3.1 L_X-L_r and L_X-L_K Relations

Fig. 2 shows that the X-ray luminosity of hot halo gas in early-type galaxies is correlated with optical luminosity with a rather large scatter.

First, we divide the large-scale environment into high ($\rho_{20}/\bar{\rho} > 20$) and low density ($\rho_{20}/\bar{\rho} \leq 20$) regions. Then we fit each subsample with a straight line given by

$$\log(L_{X,0.5-2.0\mathrm{keV}}) = A\log(L_r/10^{10.5}L_{r,\odot}) + B \quad (3)$$

using the BCES (Bivariate Correlated Error and intrinsic Scatter) bisector method (Akritas & Bershady 1996). The results are shown in Table 3. We include data with lower limits in the fit to reduce uncertainties of the parameters.

The L_X-L_r relation for galaxies with $\rho_{20}/\bar{\rho} \leq 20$ tends to be tighter and slightly steeper than counterpart in the high density region ($\rho_{20}/\bar{\rho} > 20$), consistent

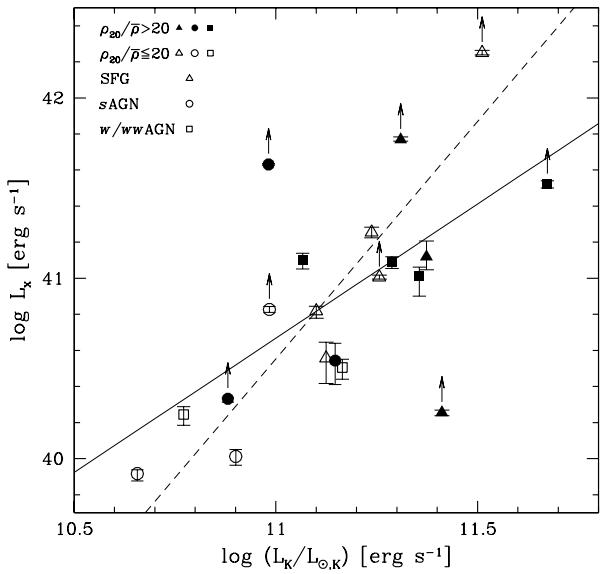

Fig. 3.— X-ray and NIR (K-band) luminosity relation for galaxies in different large-scale environment. The symbol and line notations are the same as Fig. 2.

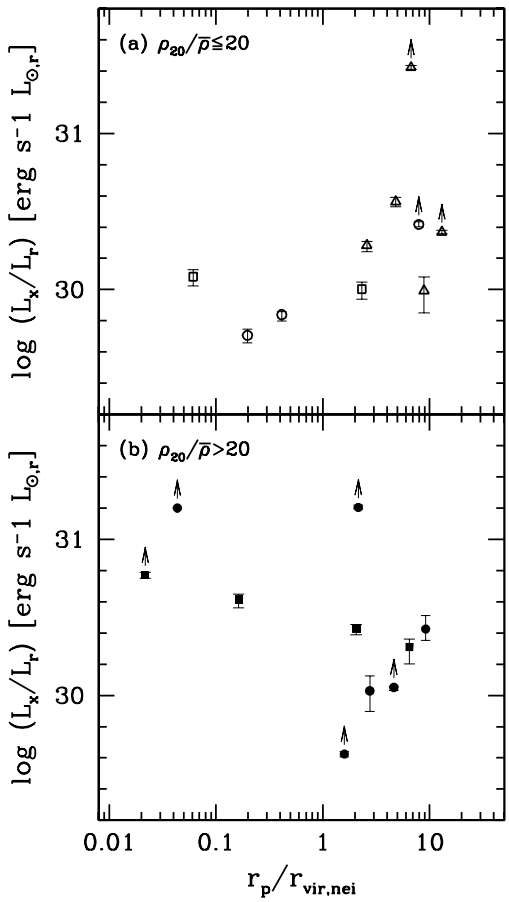

Fig. 4.— (Upper) X-ray luminosity normalized by optical (r-band) luminosity as a function of the distance to the nearest neighbor at high large-scale density regions. (Lower) The same as above, but at low large-density regions.

with the result of Mulchaey & Jeltema (2010). The correlation coefficients of the relation are 0.88 and 0.28 for the low and high density regions, respectively. The relation in the high density environment shows definitely large scatter.

To compare with other studies, we obtain the K-band luminosity of the sample galaxies from the Extended Source Catalog (XSC, Jarrett et al. 2000) of the Two Micron All Sky Survey. The correlation coefficients of the L_X and L_K relations plotted in Fig. 3 are 0.90 and 0.25 for galaxies in the low and high density regions, respectively, similar to the values found in the L_X and L_r relation. The slope of the L_X and L_K relation for galaxies in the low density region is steeper than the slope for galaxies in the high density region at 2σ significance. It clearly shows that the X-ray and NIR luminosity relation significantly differs depending on the environments where galaxies reside. Therefore, our result appears to confirm that the environment is, at least partially, responsible for the scatter seen in the relation between the X-ray and optical/NIR luminosities. The large scatter shown for galaxies in the high density environment suggests that various processes are involved in producing the thermal X-ray emission. In fact, the fitted values for the L_X-L_K relation differs from the ones obtained in Mulchaey & Jeltema (2010) and Jeltema et al. (2008). For comparison, the slope of the L_X-L_K relation for group and cluster environment is 3.92 ± 0.39 and 1.86 ± 0.23 for field galaxies. The samples they used consist of relatively nearby early-type galaxies with redshift less than 0.03 and thus are bright enough to successfully separate out the other contributions to the X-ray emission. Besides, the definition of environment they used is also different from ours. Thus the slopes obtained in Mulchaey & Jeltema and Jeltema et al. itself are not directly comparable to ours.

3.2 Environmental Effect on L_X/L_r

To obtain a deeper understanding of the various physical processes taking place in different environments, we inspect the X-ray property in the ρ_{20}-r_p parameter space shown in Fig. 4. The large-scale environment is divided into high ($\rho_{20}/\bar{\rho} > 20$) and low ($\rho_{20}/\bar{\rho} \leq 20$) density cases. We then plot the L_X scaled by L_r as a function of $r_p/r_{\rm vir,nei}$ determined by the nearest neighbor at each large-scale environment case. The figure shows that the large-scale environment is an important factor only when the target galaxy is located inside the virial radius of its neighbor ($r_p \leq r_{\rm vir,nei}$) while the dependence on the large-scale environment disappears at separations farther than the virial radius ($r_p > r_{\rm vir,nei}$), and that the effects of the nearest neigh-

bors depending on neighbor separation is critically important to the hot gas content.

In Fig. 5, upper panel (b) shows that the X-ray luminosity has a stronger correlation with the large-scale density when the distance to the nearest neighbor is smaller than the virial radius of the neighbor.

Among the six interacting galaxies with $r_p \leq r_{\rm vir,nei}$, three galaxies located in the high density regions ($\rho_{20}/\bar{\rho} \geq 20$), namely NGC4066, NGC5098, and SDSS J133110.82−014348.9, are more luminous than those in the low density regions, and their nearest neighbors also have comparable luminosity as shown in Fig. 5. Although these galaxies are experiencing close encounters with a neighbor having comparable mass in the high density region, their halos are X-ray luminous compared to those of galaxies in the lower density regions, which is contrary to the well-known effect of hot gas removal by various physical processes such as ram pressure stripping, galaxy harassment, and starvation. These galaxies are also likely to evolve through gravitational effects as they approach each other. Hence, this result suggests that for these galaxies, the removal of hot halo gas by those processes must be relatively modest and the hot halo gas is rather condensed through the accretion of intergalactic gas and confinement of outflowing gas by the ambient medium instead. This phenomenon was also found by Brown & Bregman (2000) and Sun et al. (2007). The interacting galaxies in the high density region have relatively larger L_X/L_r probably due to the additional contribution from the ambient medium and this could lead to the large scatter found in high density regions ($\rho_{20}/\bar{\rho} > 20$) shown in Fig. 2. Taking those three interacting galaxies out from the 20 galaxies makes the slopes in the L_X-L_r and L_X-L_K relations steeper, giving 2.69 ± 0.80 and 2.17 ± 0.85, respectively. These values are closer to those for the low density regions given in Table 3.

For the isolated galaxies with $r_p > r_{\rm vir,nei}$ shown in the lower panel of Fig. 5, neither ρ_{20} nor r_p depends the hot gas content. More luminous galaxies tend to have larger L_X/L_r. For these isolated galaxies, the X-ray emission depends only on the stellar content of the galaxy itself. Thus some internal processes such as stellar mass loss and continued Type Ia supernovae or AGN feedback of each galaxy could have more effect on the X-ray luminosity. Luminous galaxies having substantial dark matter halos may retain hot halos effectively while faint galaxies easily expel their hot gas.

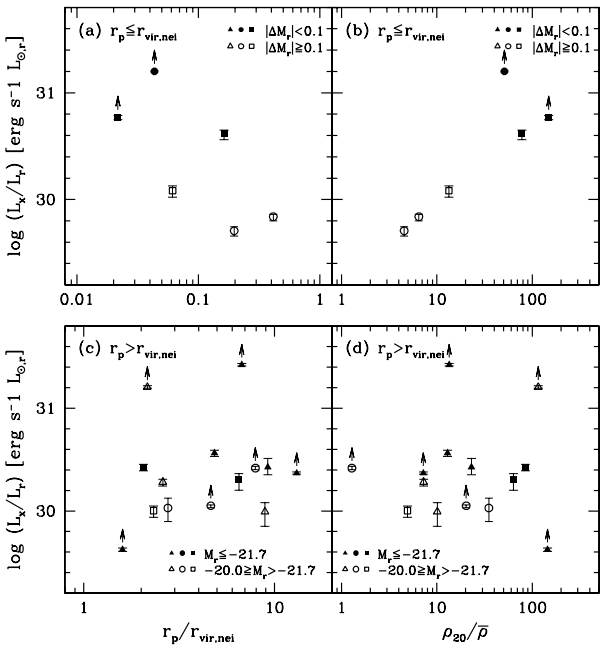

Fig. 5.— (Upper) X-ray luminosity normalized by optical (r-band) luminosity for interacting galaxies with the nearest neighbor ($r_p \leq r_{\rm vir,nei}$) as a function of the distance to the nearest neighbor (a) and as a function of the large-scale density (b). (Lower) The same as above, but for isolated galaxies ($r_p > r_{\rm vir,nei}$). ΔM in upper panels is the difference in luminosity between a target and its nearest neighbor and filled symbols are galaxies with the nearest neighbor of comparable luminosity. Samples in the lower panel are divided into two cases according to the luminosity of the target galaxy.

4. SUMMARY

We have investigated the correlation between the extended X-ray emission from the halos of optically luminous early-type galaxies and the galaxy's environments such as r_p and ρ_{20}. We cross-matched the 3rd Data Release of the Second *XMM-Newton* Serendipitous Source Catalog to a volume-limited sample of the Sloan Digital Sky Survey Data Release 7 with $M_r < -19.5$ and $0.020 < z < 0.085$ which was generated from the KIAS value-added catalog (Choi et al. 2010). We obtained 20 early-type galaxies with reliable X-ray signals from the positional cross-matching between the two data sets. Although the small size of the sample more or less limited the scope of issues, it was still useful to draw obvious results.

The X-ray luminosity of the galaxy was found to have a tighter correlation with the optical and NIR luminosities for galaxies with large-scale background density of $\rho_{20}/\bar{\rho} \leq 20$ than for those with $\rho_{20}/\bar{\rho} > 20$. Furthermore, the X-ray to optical (r-band) luminosity ratio, L_X/L_r, shows a clear dependence on the distance to the nearest neighbor, r_p, and on the large-scale density environment, ρ_{20}, only where the galaxies in pair interact hydrodynamically, $r_p < r_{\rm vir}$. These results lead us to conjecture that the galaxies in the high local density region have other mechanisms that are responsible for their halo X-ray luminosities than the current presence of a close encounter, or alternatively, the cooling time of the heated gas halo is longer than the typical time between the subsequent encounters in the high local density region so that L_X/L_r is rather

insensitive to the current presence of a close encounter (r_p) and to the expected time after the last encounter (ρ_{20}).

eROSITA, the extended Roentgen Survey with an Imaging Telescope Array (Predehl et al. 2012), is planned for launch in the year 2014 and will scan the entire sky for four years. Its sensitivity will be approximately 20 times the Roentgen Satellite (ROSAT), and the data from this mission will drastically increase the number of galaxy samples with X-ray emitting halos, and a study like the present one here will benefit from these new data.

ACKNOWLEDGMENTS

Support for this work was provided by the National Research Foundation of Korea to the Center for Galaxy Evolution Research (No. 2010-0027910). S.S.K. was supported by Mid-career Reaserch Program (No.2011-0016898) through the National Research Foundation (NRF) grant funded by the Ministry of Education, Science and Technology (MEST) of Korea.

Funding for the SDSS and SDSS-II has been provided by the Alfred P. Sloan Foundation, the Participating Institutions, the National Science Foundation, the U.S. Department of Energy, the National Aeronautics and Space Administration, the Japanese Monbukagakusho, the Max Planck Society, and the Higher Education Funding Council for England. The SDSS Web site is http://www.sdss.org/.

This research is based on observations obtained with XMM-Newton, an ESA science mission with instruments and contributions directly funded by ESA member states and the USA (NASA).

This publication makes use of data products from the Two Micron All Sky Survey, which is a joint project of the University of Massachusetts and the Infrared Processing and Analysis Center/California Institute of Technology, funded by the National Aeronautics and Space Administration and the National Science Foundation.

REFERENCES

Abazajian, K. N., et al. 2009, The Seventh Data Release of the Sloan Digital Sky Survey, ApJS, 182, 543

Akirtas, M. G., & Bershady, M. A. 1996, Linear Regression for Astronomical Data with Measurement Errors and Intrinsic Scatter, ApJ, 470, 706

Blanton, M. R., et al. 2003, Estimating Fixed-Frame Galaxy Magnitudes in the Sloan Digital Sky Survey, ApJ, 125, 2348

Baldwin, J. A., Phillips, M. M., & Terlevich, R. 1981, Classification Parameters for the Emission-Line Spectra of Extragalactic Objects, PASP, 93, 5

Boroson, B., Kim, D.-W., & Fabbiano, G. 2011, Revisiting with *Chandra* the Scaling Relations of the X-Ray Emission Components Binaries, Nuclei and Hot Gas of Early-Type Galaxies, ApJ, 729, 12

Bregman, J. N., & Parriott, J. R. 2009, Mass Loss from Planetary Nebulae in Elliptical Galaxies, ApJ, 669, 923

Brown, B. A., & Bregman, J. N. 1998, X-Ray Emission from Early-Type Galaxies: A Complete Sample Observed by ROSAT, ApJ, 495, L75

Brown, B. A., & Bregman, J. N. 2000, The Effect of Environment on the X-Ray Emission from Early-Type Galaxies, ApJ, 539, 592

Canizares, C. R., Stewart, G. C., & Fabina, A. C. 1983, Radiative Accretion of Intracluster Gas onto Dominant Galaxies in Poor Clusters, ApJ, 272, 449C

Canizares, C. R., Fabbiano, G., & Trinchieri, G. 1987, Properties of the X-Ray Emitting Gas in Early-Type Galaxies, ApJ, 312, 503

Choi, Y.-Y., Han, D.-H., & Kim, Sungsoo. S. 2010, Korea Institute for Advanced Study Value-Added Catalog, JKAS, 43, 191

Ellis, S. C., & O'Sullivan, E. 2006, Correlations of Near-Infrared, Optical and X-Ray Luminosity for Early-Type Galaxies, MNRAS, 367, 627

Eskridge, P. B., Fabbiano, G., & Kim, D.-W. 1995, A Multiparametric Analysis of the Einstein Sample of Early-Type Galaxies. 1: Luminosity and ISM Parameters, ApJS, 97, 141

Fabbiabo, G., & Trinchieri, G. 1985, A Statistical Analysis of the Einstein Normal Galaxy Sample. I. Spiral and Irregular Galaxies, ApJ, 296, 430

Forman, W., Jones, C., & Tucker, W. 1985, Hot Coronae around Early-Type Galaxies, ApJ, 293, 102

Helsdon, S. F., Ponman, T. J., O'Sullivan, E., & Forbes, D. A. 2001, X-Ray Luminosities of Galaxies in Groups, MNRAS, 325, 693

Hwang, H. S., & Park, C. 2009, Evidence for Morphology and Luminosity Transformation of Galaxies at High Redshifts, ApJ, 700, 791

Hwang, H. S., & Park, C. 2010, Orbital Dependence of Galaxy Properties in Satellite Systems of Galaxies, ApJ, 720, 522

Hwang, H. S., Elbaz, D., & Lee, J. C. 2010, Environmental Dependence of Local Luminous Infrared Galaxies, A&A, 522, A33

Hwang, H. S., Elbaz, D., Dickinson, M., Charmandaris, V., & Daddi, E. 2011, GOODS-Herschel: the Impact of Galaxy-Galaxy Interactions on the Far-Infrared Properties of Galaxies, A&A, 535, A60

Irwin, J. A., Bregman, J. N., & Athey, A. E. 2004, The Lack of Very Ultraluminous X-Ray Sources in Early-Type Galaxies, ApJ, 601, L143

Jarrett, T. H., Chester, T., Cutri, R., Schneider, S., Skrutsie, M., & Hchra, J. P. 2000, 2MASS Extended Source Catalog: Overview and Algorithms, AJ, 119, 2498

Jeltema, T. E., Binder, B., & Mulchaey, J. S. 2008, The Hot Gas Halos of Halos of Galaxies in Groups, ApJ, 679, 1162

Kim, D.-W., Fabbiano, G., & Trichieri, G. 1992, The X-Ray Spectra of Galaxies. II. Average Spectral Properties and Emission Mechanisms, ApJ, 393, 134

Kim, D.-W., & Fabbiano, G. 2010, X-Ray Properties of Young Early-Type Galaxies: I. X-Ray Luminosity Function of Low Mass X-Ray Binaries, ApJ, 721, 1523

Kauffmann, G., et al. 2003, The Host Galaxies of Active Galactic Nuclei, MNRAS, 346, 1055

Li, J.-T., Wang, Q. D., Li, Z., & Chen, Y. 2011, Dynamic S0 Galaxies. II. The Role of Diffuse Hot Gas, ApJ, 737, 41

Mathews, W. G. 1990, Interstellar Events in Elliptical Galaxies, ApJ, 354, 468

Mathews, W. G., & Brighenti, F. 2003, Hot Gas in and around Elliptical Galaxies, ARA&A, 41, 191

Memola, E., Trinchieri, G., Wolter, A., Focardi, P., & Kelm, B. 2009, The Divers X-Ray Properties of Four Truly Isolated Elliptical Galaxies: NGC2954, NGC6172, NGC 7052 and NGC 7785, A&A, 497, 359

Mulchaey, J. S., & Jeltema, T. E. 2010, Hot Gas Halos in Early-Type Field Galaxies, ApJ, 715, L1

O'Sullivan, E., Forbes, D. A., & Ponman, J. T. 2001, A Catalogues and Analysis of X-Ray Luminosity of Early-Type Galaxies, MNRAS, 328, 461

Park, C., Gott, J. R., & Choi, Y.-Y. 2008, Transformation of Morphology and Luminosity Classes of the SDSS Galaxies, ApJ, 674, 784

Park, C., & Choi, Y.-Y. 2009, Combined Effects of Galaxy Interactions and Large-Scale Environment on Galaxy Properties, ApJ, 691, 1828

Predehl, P., et al. 2012, eROSITA, SPIE Conference Proceeding, 8443, 84431R

Rasmussen, J., Bai, X.-N., Mulchaey, J., van Gorkom, J. H., & Jeltema, T. E. 2012, Hot and Cold Galactic Gas in the NGC 2563 Galaxy Group, ApJ, 747, 31

Schlegel, D. J., Finkbeiner, D. P., & Davis, M. 1998, Maps of Dust Infrared Emission for Use in Estimation of Reddening and Cosmic Microwave Background Radiation Foregrounds, ApJ, 500, 525

Sun, M., Jones, C., Forman, W., Vikhlinin, A., Donahue, M., & Voit, M. 2007, X-Ray Thermal Coronae of Galaxies in Hot Clusters: Ubiquity of Embedded Mini-Cooling Ocres, ApJ, 657, 197

Silverman, J. D., et al. 2005, Hard X-Ray-Emitting Active Galactic Nuclei Selected by the *Chandra* Multiwavelength Project, ApJ, 618, 123

Sun, M. 2009, Every BCG with a Strong Radio Agn has an X-Ray Cool Core: Is the Cool Core-Noncool Core Dichotomy Too Simple?, ApJ, 704, 1586

Tegmark, M., Blanton, M. R., Strauss, M. A., Hoyle, F., & Schlegel, D. 2004, The Three-Dimensional Power Spectrum of Galaxies from the Sloan Digital Sky Survey, ApJ, 606 ,702

Trinchieri, G., & Fabbiano, G. 1985, A Statistical Analysis of the Einstein Normal Galaxy Sample - Part Two - Elliptical and S0 Galaxies, ApJ, 296, 447

Turner, T. J., & Pounds, K. A. 1989, The EXOSAT Spectral Survey of AGN, MNRAS, 240, 833

Watson, M. G., Schroder, A. C., Fyfe, D., Page, C. G., & Lamer, G. 2008, The XMM-Newton Serendipitous Survey V. The Second XMM-Newton Serendipitous Source Catalogue, A&A, 493, 339

White, S. D. M., & Frenk, C. S. 1991, Galaxy Formation through Hierarchical Clustering, ApJ, 379, 52

York, D., et al. 2000, The Sloan Digital Sky Survey: Technical Summary, AJ, 120, 1579